Direct Conversion of 5-Hydroxymethylfurfural to Furanic Diether by Copper-Loaded Hierarchically Structured ZSM-5 Catalyst in a Fixed-Bed Reactor

Hualei Hu[+],[a] Tingting Xue[+],[a, b] Zhenxin Zhang,[a, c] Jiang Gan,[a, c] Liangqi Chen,[a, b] Jian Zhang,*[a, c] Fengzuo Qu,[b] Weijie Cai,*[b] and Lei Wang*[a, d]

The highly-efficient conversion of 5-hydroxymethylfurfural (HMF) to 2,5-bis(ethoxymethyl)furan (BEMF) was achieved over the copper-loaded hierarchically structured ZSM-5 (Cu/HSZ) catalysts in the continuous fixed-bed reactor. The main reaction path for BEMF synthesis on the Cu/HSZ catalysts was confirmed as following: HMF was firstly hydrogenated to BHMF intermediates over metal sites and then the formed BHMF was etherified by acid sites. Benefiting from the ammonia evaporation (AE) method promoted the dispersion of copper and reduced the acidity, the Cu/HSZ-AE catalyst exhibited more excellent BEMF yield and stability than the catalyst prepared by conventional incipient-wetness impregnation (Cu/HSZ-IW). Indeed, the inactivation of Cu/HSZ-IW catalyst was mainly attributed to the deactivation of copper by carbon species deposition.

Introduction

With the depletion of fossil resources and the serious environmental pollution, utilization of renewable biomass resources to produce the valuable fuels and chemicals has received growing interests.[1] 5-Hydroxymethylfurfural (HMF), obtained from biomass-derived sugars via dehydration, has been identified as the key platform compound for synthesis of 2,5-furandicarboxylic acid (FDCA), levulinic acid (LA), furanic ethers, and other high-valued chemicals.[2] Among them, furanic ethers have drawn considerable attention in recent years considering their high energy density, high cetane number, and suitable fuel blending properties.[3] Currently, most of the literature has focused on the etherification of HMF with alcohols to produce 5-(alkoxymethyl) furfural (AMF).[4] However, the remained aldehyde functional group significantly reduces its molecule stability.[5] To overcome this drawback, some researchers hydrogenating HMF to 2,5-bis (hydroxymethyl)furan (BHMF) and then etherifying BHMF with alcohols to produce 2,5-bis(alkoxymethyl)furans (BAMF).[6] As compared with the mono-ether AMF, the diether BAMF possess the higher stability of the molecular structure as well as the wider carbon number range and application fields.[5]

So far, the two-step route, i.e., the isolated HMF hydrogenation and BHMF etherification process, had been widely investigated over various heterogeneous catalysts.[7] For instance, Chatterjee et al.[7a] used the Pt/MCM-41 as catalyst for HMF hydrogenation, obtaining 98.9% yield of BHMF under 0.8 MPa of H_2 at 35 °C for 2 h. Han et al.[7b] reported that the Ru(OH)x/ZrO_2 catalyst gave 99% yield of BHMF under 1.5 MPa of H_2 at 120 °C for 2 h. Balakrishnan et al.[7c] tested the performance of Amberlyst-15 in etherification of BHMF with ethanol, in which a 80% yield of 2,5-bis(ethoxymethyl)furan (BEMF) was achieved after reaction at 40 °C for 16 h. Musolino et al.[7d] demonstrated that the acid purolite could efficiently accelerate the etherification of BHMF, leading to a 99% yield of BEMF under mild conditions (at 40 °C for 24 h). In our previous work, the potassium-doped Cu/Al_2O_3 catalyst was found to exhibit superior performance in selective hydrogenation of HMF and a 98.9% yield of BHMF was achieved in fixed bed reactor under 2.0 MPa of H_2 at 120 °C.[8] Moreover, the hierarchically structured ZSM-5 zeolites (HSZ) was applied in our group for the etherification of BHMF with ethanol, obtaining 94.7% and 90.4% yield of BEMF in the batch and fixed bed reactors, respectively.[9] However, as for the two-step route, heavy costs incurred in the intermediate product separation and purification is unavoidable, which restrict its pilot-scale application to some extent.

The direct conversion of HMF to BAMF (i.e., one-step route) could avoid the tedious purification steps and thus help to reduce the energy consumption, cost operation and waste emission, thereby resulting in a green and sustainable synthesis process.[10] Nowadays, only few works have been conducted on the direct production of BAMF from HMF under hydrogen atmosphere. Balakrishnan et al.[7c] combined the Pt/Al_2O_3 and

[a] Dr. H. Hu,[+] T. Xue,[+] Z. Zhang, J. Gan, L. Chen, Prof. J. Zhang, Prof. L. Wang
Ningbo Institute of Materials Technology & Engineering
Chinese Academy of Sciences
1219 Zhongguan West Road
Ningbo 315201 (P. R. China)
E-mail: jzhang@nimte.ac.cn
wanglei@nimte.ac.cn
[b] T. Xue,[+] L. Chen, Prof. F. Qu, Prof. W. Cai
Dalian Polytechnic University
No. 1st Qinggongyuan
Ganjingzi, Dalian 116034 (P. R. China)
E-mail: caiwj@dlpu.edu.cn
[c] Z. Zhang, J. Gan, Prof. J. Zhang
University of Chinese Academy of Sciences
No.19(A) Yuquan Road, Shijingshan District
Beijing 100049 (P. R. China)
[d] Prof. L. Wang
Zhejiang Sugar Energy Technology Co. Ltd.
1818 Zhongguan West Road
Ningbo 315201 (P. R. China)
[+] These authors contributed equally to this work.

Supporting information for this article is available on the WWW under https://doi.org/10.1002/cctc.202100489

Amberlyst-15 catalysts for hydrogenation and etherification in one batch reactor, in which only 59% yield of BEMF was achieved at 60 °C for 18 h under 1.38 MPa H_2. Cao et al.[6a] used Cu/SiO_2 and ZSM-5 as the catalysts for 2,5-bis(methoxymethyl) furan (BMMF) synthesis and 68% yield of BMMF was observed after reaction at 120 °C for 12 h under 2.5 MPa H_2. In contrast to the physical combination of two different catalysts, using bifunctional catalyst (containing two types of active components within nanoscale distances) could enable the reaction more successively and efficiently in the catalysis cascade.[11] Wei et al.[12] used the Cu-USY bifunctional catalyst for conversion of HMF to BMMF. Unfortunately, only 11.4% yield of BMMF was achieved due to the unsatisfactory catalyst activity. Therefore, it is urgent to develop efficient and stable bifunctional catalyst for the direct transformation of HMF to furanic diether. Moreover, most of research work conducted the reaction in the batch reactor. In contrast, the continuous operation in the fixed-bed reactor is more efficient and more advantageous for the large-scale industrial production.[13]

In this work, the copper-loaded HSZ bifunctional catalyst was prepared via the incipient-wetness impregnation (IW) and ammonia evaporation (AE) method, respectively. The effect of copper loading on the physicochemical properties of the bifunctional catalysts was systemic characterized. By evaluating the catalytic performance of bifunctional catalysts in the fixed bed reactor, the role of metal and acid sites in the hydrogenation-etherification process was investigated in detail to propose the reaction path.

Results and Discussion

Figure 1a shows the XRD patterns of the synthesized HSZ support and Cu/HSZ catalysts. The diffraction patterns of the HSZ were consistent with the reported MFI-structured materials and no other diffraction peaks could be detected, indicating that the synthesized HSZ sample was the pure MFI-type zeolite.[14] All of the Cu/HSZ catalysts exhibited the similar diffraction peaks to HSZ sample, implying that the framework structure of HSZ was maintained after the copper loading. Moreover, no diffraction peaks corresponding to CuO could be observed on the Cu/HSZ catalysts, which might be ascribed to its higher dispersion in HSZ crystals or the small particles below the detection limit of XRD.[8,15]

Figure 1b shows the N_2 physisorption-isotherms of the as-prepared catalysts. It can be seen that all of the samples showed the type-IV hysteresis loop, which was associated with the capillary condensation of the probe molecule in mesopores.[16] Moreover, the BJH pore size distribution of these samples was given in Figure 1b insert. Both the HSZ sample and copper-loaded HSZ catalysts possessed the similar pore size distribution (3 ~ 100 nm). As listed in Table 1, the micropores and mesopores volume of HSZ sample was 0.097 $cm^3 \cdot g^{-1}$ and 0.36 $cm^3 \cdot g^{-1}$, confirming that the synthesized HSZ sample was hierarchically structured ZSM-5 zeolites. As for the Cu/HSZ-IW prepared by incipient-wetness impregnation, both the micropores and mesopores volume was slightly lower than that of the HSZ sample, which could be attributed to that the partially pore was blocked by the copper component.[17] While for the

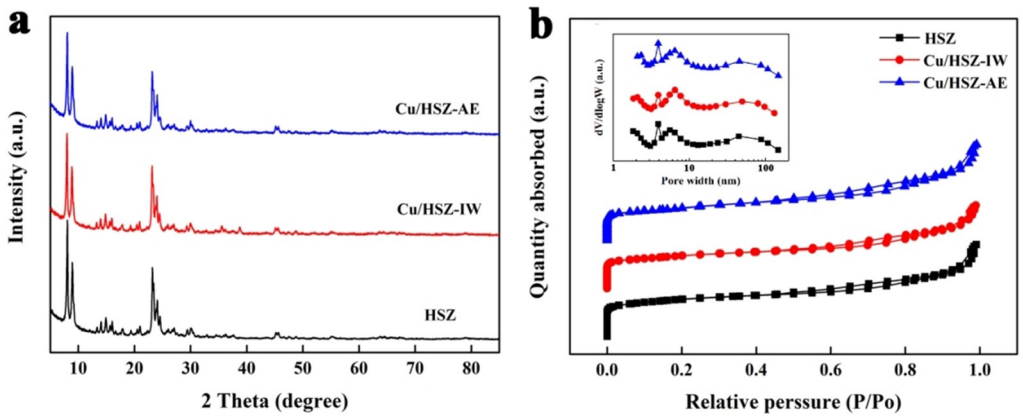

Figure 1. XRD patterns (a), N_2 adsorption-desorption isotherms (b), and pore size distribution (inset) of the samples.

Table 1. Chemical compositions and physicochemical properties of the samples.

Sample	Si/Al moral ratio[a]	Cu [wt%][a]	Cu [wt%][b]	Surf. Cu [wt%][c]	S_{BET} [$m^2 \cdot g^{-1}$][d]	V_{micro} [$cm^3 \cdot g^{-1}$][e]	V_{meso} [$cm^3 \cdot g^{-1}$][f]	D_{Cu} [%][g]	S_{Cu} [m^2/g][f]	d_{Cu} [nm][g]	X_{Cu0} [%][h]
HSZ	102.1	0	0	0	417	0.097	0.36	/	/	/	/
Cu/HSZ-IW	101.3	5.15	5.01	9.72	371	0.084	0.33	35.4	229.7	2.82	45.0
Cu/HSZ-AE	96.8	5.30	4.92	15.0	378	0.077	0.39	43.3	280.9	2.30	45.5

[a] Calculated by XRF. [b] Calculated by ICP-OES. [c] Calculated by XPS. [d] Determined by BET method. [e] Estimated using the t-plot method. [f] Determined by a subtraction of total pore volume at a relative pressure of $P/P_0 = 0.99$ from the microporous pore volume obtained from the t-plot. [g] Copper dispersion, exposed metallic copper surface area, and copper particle size were calculated by N_2O adsorption-decomposition.[h] Intensity ratio between Cu^0 and ($Cu^+ + Cu^0$) by deconvolution of Cu LMM XAES.

Cu/HSZ-AE sample, although the volume of micropores decreased to 0.077 $cm^3 \cdot g^{-1}$, the mesopores volume increased to 0.39 $cm^3 \cdot g^{-1}$. This could be ascribed to that a part of framework siliceous species was extracted by the alkaline ammonia solution, which in turn generated the additional mesopores at the expense of micropores.[18] This also well explained the decline of diffraction peaks intensity and Si/Al ratio of Cu/HSZ-AE catalyst.

Figure 2 gives the SEM and TEM images of the synthesized HSZ samples. As seen in Figure 2a and 2b, the HSZ sample exhibited a regular ellipsoidal shape with a particle size of about 200~500 nm. Moreover, numerous cavities could be observed on their surfaces. The TEM images depicted that these ellipsoidal particles were formed by the aggregation of crystalline nanoparticles. Thus, the additional mesoscale porosity was created between these nanoparticles.[16]

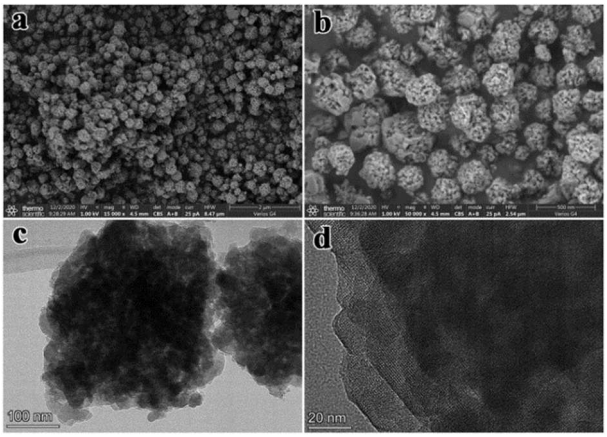

Figure 2. SEM (a–b) and TEM (c–d) images of the HSZ samples.

NH_3-TPD and Py-IR were performed to investigate the acidic properties of the samples. As shown in Figure 3a, the NH_3-TPD profiles of the synthesized HSZ sample exhibited three peaks, denoted as low-temperature, middle-temperature, and high-temperature peaks, which could be attributed to the ammonia molecules absorbed on the weak, moderate, and strong acid sites, respectively.[19] In contrast, the peak temperature of strong acid sites on the reduced Cu/HSZ samples was obviously lower, suggesting that the loading of copper led to the greatly decrease in the acid strength. This might be due to the interaction of the surface acid sites and the introduced copper species.[20] In addition, it was also noted that the amount of moderate acid sites on the Cu/HSZ catalysts remarkably increased, which led to the increase in total acid amount (Table 2). According to the literature, the copper species could adsorb the ammonia molecules and then desorb sequentially.[21] Thus, the increase in the acid sites amount observed on the Cu/HSZ catalysts was reasonable. As compared to the Cu/HSZ-IW catalyst, both the strength and amount of acid sites on the Cu/HSZ-AE sample was relatively lower, which could be attributed to that the leaching of framework siliceous species in the

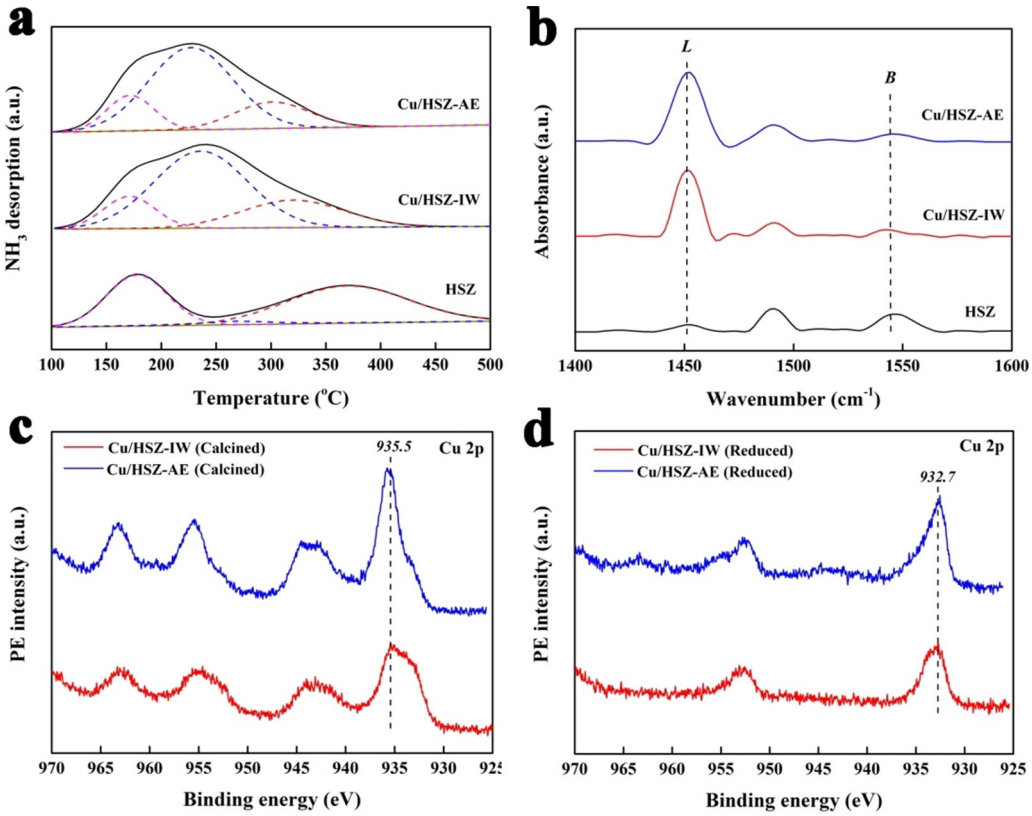

Figure 3. NH_3-TPD (a), Py-IR (b) and Cu 2p XPS spectra (c and d) of the samples.

Table 2. Surface acid properties of the HSZ and Cu/HSZ samples.

Catalyst	Number of acid sites (mmol of NH_3 g^{-1})[a] weak (< 200 °C)	moderate (200 ~ 300 °C)	strong (> 300 °C)	Total acid	Ratio of B/L[b]	Brønsted acid[c]	Lewis acid[c]
HSZ	0.42	0.05	0.63	1.10	5.63	0.93	0.17
Cu/HSZ-IW	0.22	1.00	0.38	1.60	0.18	0.24	1.36
Cu/HSZ-AE	0.23	0.94	0.28	1.45	0.15	0.19	1.26

[a] Calculated by NH_3-TPD. [b] Determined by Py-IR. [c] Number of Brønsted and Lewis acid were calculated by the ratio of B/L and the total amount of acid sites, which determined by Py-IR and NH_3-TPD, respectively.

ammonia-evaporation method also reduced the amount of framework aluminum species being responsible for the formation of acid sites.[22]

Figure 3b shows the Py-IR spectra of the samples. The bands at 1545 cm^{-1} and 1454 cm^{-1} were ascribed to the adsorptions of pyridine on the Brønsted and Lewis acid sites, respectively.[23] It can be seen that the amount ratio of Brønsted acid sites to Lewis acid sites (abbreviated as B/L) of the HSZ sample was 5.63 (Table 2), indicating that the aluminum species on the synthesized HSZ sample mainly existed as the coordinatively saturated sites (Brønsted acid). With the introduction of copper, the band intensity assigned to Brønsted acid decreased, while the band intensity assigned to Lewis acid significantly increased, which might be due to that some Brønsted acid sites of zeolite were converted to Lewis acid by exchanged with Cu^{2+}.[24] This also led to the dramatically declined in B/L ratio of Cu/HSZ catalysts. In addition, this phenomenon further confirmed the interaction of surface acid sites and copper species from the other side.

The chemical states of copper over the calcined and reduced Cu/HSZ catalysts were detected via XPS technique. In contrast to the calcined samples, the spectra peaks at 940–945 eV and 960–965 eV disappeared in the reduced samples. Meanwhile, the peak at a binding energy of 935.5 eV was shifted to about 932.7 eV, meaning that the Cu^{2+} on the Cu/HSZ catalysts had been reduced to Cu^{+} or Cu^{0} during the reduction process.[25] In order to discriminate the Cu^{+} species from Cu^{0} species, the Cu LMM XAES spectra were collected (Figure 1S). The XAES profiles were split into two symmetrical peaks centered at about 914.0 and 917.0 eV, corresponding to Cu^{+} and Cu^{0} species, respectively, indicating that both Cu^{0} and Cu^{+} coexisted on the surface of the reduced Cu/HSZ catalysts.[26] Moreover, the percentage of Cu^{0} on the Cu/HSZ-IW and Cu/HSZ-AE catalyst was similar (Table 1).

The dark-field TEM images and relevant particle size distributions of the reduced Cu/HSZ samples are shown in Figure 4. It can be seen that in all cases, the copper particles were uniformly dispersed on the HSZ support. In contrast, the average size of the copper particles on Cu/HSZ-AE (2.25 nm) was lower than that of Cu/HSZ-IW (2.80 nm), which was consistent with the copper dispersion measured by N_2O adsorption-decomposition (Table 1). This finding indicated that using the ammonia-evaporation method could facilitate the formation of copper particles with smaller size. The reason might be attributed to that the strong interaction between the copper species and HSZ support prevented the transmigration

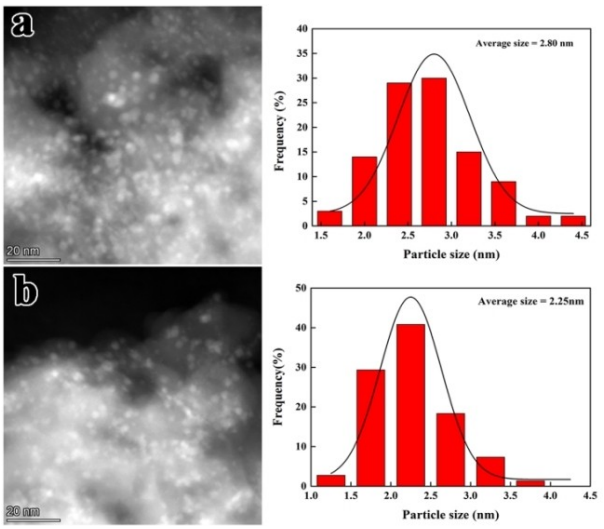

Figure 4. HAADF/STEM images (left) and the relevant particle size distributions (right) of the reduced Cu/HSZ-IW (a) and Cu/HSZ-AE (b) samples.

and sintering of copper particles during thermal treatment process.[27]

H_2-TPR was conducted to investigate the reduction behavior of the Cu/HSZ catalysts. As shown in Figure 5, the reduction peaks in the range of temperature 140–220 °C were observed on Cu/HSZ samples, which could be ascribed to the reduction of CuO.[8] On the other hand, a reduction peak at the temperature of 184 °C was noted for the Cu/HSZ-IW sample. As for the

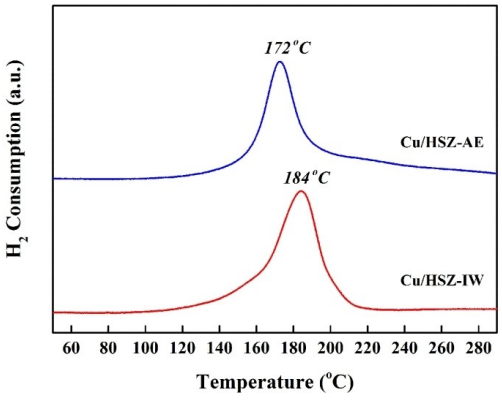

Figure 5. H_2-TPR profiles of Cu/HSZ samples synthesized by different methods.

Cu/HSZ-AE sample, the reduction peaks shifted to 172 °C, suggesting that the CuO species on the Cu/HSZ-AE sample were relatively easier to be reduced than the Cu/HSZ-IW sample. It is well known that as compared to the bulk CuO particles, the highly dispersed copper species can be more easily reduced because of their relatively higher surface area exposed to H_2.[28] As suggested by TEM and N_2O adsorption-decomposition, the Cu/HSZ-AE sample possessed the smaller average size of copper particles and higher copper dispersion, thereby resulting in the decrease of reduction temperature.

In order to check the distribution of copper nanoparticles on the HSZ support, the ICP-OES, XRF, and XPS were used. As seen in Table 1, the copper content detected by the ICP-OES and XRF was closer to the nominal value. In contrast, the content of surface copper calculated from the intensities of signals in XPS spectra was significantly higher, indicating that the copper species was favored to distribute on the outer surface of the HSZ support.[29]

Figure 6 gives the catalytic performance of the synthesized HSZ catalyst and Cu/HSZ catalysts in the direct conversion of HMF to BEMF. As shown in Figure 6a, the conversion of HMF over the HSZ increased to 75.4% at the first 1.5 h and then maintained at about 77.0% in the next 6.5 h. In comparison with HSZ support, the Cu/HSZ-IW and Cu/HSZ-AE catalysts exhibited higher catalytic activity, obtaining about 98.4% and 99.3% conversion of HMF at 1.5 h, respectively. With further increasing the reaction time, the HMF conversion of Cu/HSZ-IW catalyst slowly decreased to 93.9%, indicating the gradual catalyst deactivation during the reaction. While for the Cu/HSZ-AE catalyst, the conversion of HMF was still maintained at above 99.0%. The result depicted that the Cu/HSZ-AE catalyst in the direct conversion of HMF was more stable than the Cu/HSZ-IW catalyst.

The BEMF yield on the different catalysts was displayed in Figure 6b. It can be seen that the yield of BEMF on the HSZ catalyst was lower than 3.5% all along, indicating that HMF was mainly converted into other products. For the Cu/HSZ catalysts, the yield of BEMF increased during the first 1.5 h and reached a maximum of 77.1%. However, in the subsequent time, the two Cu/HSZ catalysts exhibited the significant difference in the trend of BEMF yield. For the Cu/HSZ-IW, the BEMF yield sharply decreased to 63.3%, while the Cu/HSZ-AE catalyst maintained at about 80.0% yield of BEMF. This clearly indicated the higher stability of Cu/HSZ-AE catalyst.

In order to investigate the reason for the high BEMF yield obtained over the Cu/HSZ-AE catalyst as well as its high stability, it is necessary to understand the conversion path of HMF and the role of copper and acid sites. In general, HMF could be converted to the targeted product BEMF via the reaction path as follows (Figure 7): a) HMF was firstly hydrogenated into BHMF by the metal sites and then BHMF was etherified with ethanol over the acid sites to produce EMFA and BEMF in sequence. b) HMF was etherified into EMF by the acid sites, and the formed EMF was then hydrogenated into EMFA over the metal sites. Finally, the EMFA was further etherification with ethanol to produce BEMF. c) HMF was firstly hydrogenated into BHMF by the acid catalyzed Meerwein-Ponndorf-Verley (MPV) reaction. Then, the formed BHMF was converted to BEMF via the acid-catalyzed etherification.[3,12]

With the aim to verify the specific reaction path, the performance of Cu/HSZ-AE catalyst was evaluated under the nitrogen atmosphere. In this case, BHMF could not be formed via the copper catalyzed hydrogenation of HMF with hydrogen. As shown in Figure 2S, the maximum HMF conversion and BEMF yield on the Cu/HSZ-AE catalyst was only about 72.7% and 20.5%, respectively. Moreover, upon increasing reaction time, the yield of BEMF rapidly decreased to 6.2%. This suggested that the Cu/HSZ-AE catalyst could indeed facilitate the conversion of HMF to BHMF via the MPV reaction, but it might not be the main reaction path for the synthesis of BEMF.

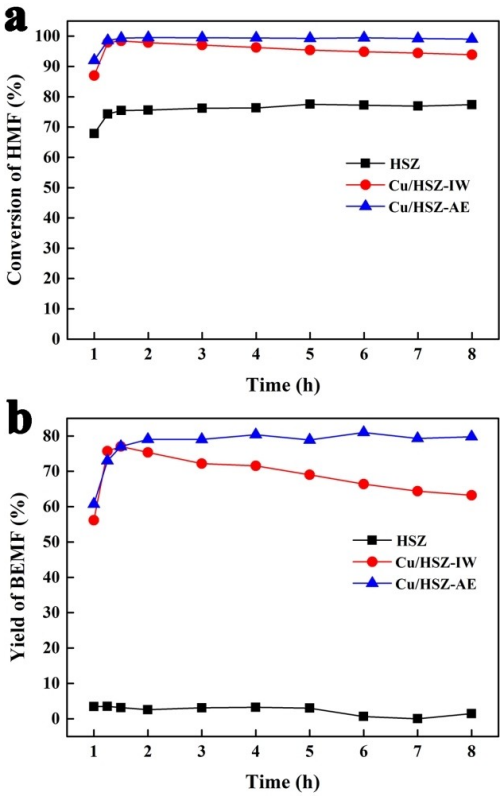

Figure 6. Catalytic performances of the HSZ and Cu/HSZ catalysts in the direct conversion of HMF to BEMF. (Reaction conditions: 1.0 g catalyst, 2.0 g L^{-1} HMF/ethanol, WHSV of HMF = 0.05 h^{-1}, 2.0 MPa H_2, and 140 °C.

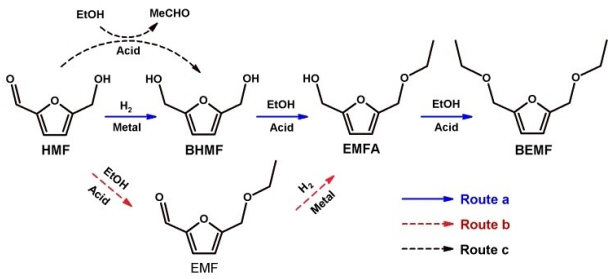

Figure 7. Proposed reaction pathways for the conversion of HMF to BEMF.

Table 3. The activity and selectivity of HSZ and Cu/HSZ catalysts in the direct conversion of HMF to BEMF.

Catalyst	Raw material	Conversion [%]	Selectivity [%] BEMF	EMFA	BHMF	EMF	EMFDEA	HMFDEA	ROP	THP	unknown
HSZ	HMF	77.4	1.9	4.4	/	68.3	2.6	17.3	/	/	5.5
Cu/HSZ-IW	HMF	93.9	67.4	2.6	/	3.6	/	4.8	13.5	3.1	5.0
Cu/HSZ-AE	HMF	99.0	80.6	1.8	/	/	/	2.1	6.5	1.8	8.0
Cu/HSZ-AE	HMF(N_2)	65.5	9.5	3.3	11.4	4.4	14.4	46.4	/	/	10.6

Reaction conditions: 1.0 g catalyst, 2.0 g L^{-1} HMF/ethanol, WHSV of HMF = 0.05 h^{-1}, 2.0 MPa H_2, 140 °C, 8 h.

According to the literature, both the Brønsted acid sites and Lewis acid sites could catalyze the etherification reaction, but only the Lewis acid sites could catalyze the MPV reaction.[3] Although the introduction of copper significantly increased the amount of Lewis acid sites, the MPV reaction was promoted slightly, suggesting that the introduced Lewis acid sites was not highly active for this reaction. The reason could be ascribed to that the strength of these Lewis acid sites was lower than the Lewis acid sites formed by framework Sn or Zr.[3b] Moreover, in the reductive etherification of HMF, the MPV conversion of HMF to BHMF is the rate-determining step.[5a] In this case, the contact time of the formed BHMF and acid sites was further shortened, which led to the presence of BHMF in the product. Then, the performance of Cu/HSZ-AE catalyst were further tested in EMF conversion (Figure 3S). It can be seen that although the conversion of EMF could be reached to above 90%, no BEMF was generated and the yield of EMFA was lower than 2.0% all along, indicating that the Cu/HSZ-AE catalyst could not effectively produce the BEMF from HMF via the intermediate EMF. Based on the above results, it was reasonable to propose that the main reaction path for the synthesis of BEMF over the Cu/HSZ-AE catalyst was route a, i.e., HMF was firstly hydrogenated overactive copper species and then the formed BHMF was etherified by acid sites.

The product selectivity of the HSZ and Cu/HSZ catalysts are listed in Table 3. For the HSZ catalyst, the selectivity of EMF and 5-(hydroxymethyl)-furfural diethyl acetal (HMFDEA) was reached to 68.3% and 17.3%, respectively, which should be ascribed to that the catalyst only possessed the acid sites. While for the Cu/HSZ catalysts, HMF could be effectively converted into BEMF. As compared to the HSZ catalyst, the selectivity of ring-opening products (ROP) and transitional hydrogenation products (THP) on the Cu/HSZ catalysts was significantly higher, suggesting that the side reactions such as transitional hydrogenation, hydrogenolysis, and ring-opening was indeed promoted by the coexistence of copper and acid sites.[8,30] The other direct evidence was that when using the nitrogen as carrier gas, in which the hydrogenation performance of copper sites was suppressed, the ROP and THP products were not detected over the Cu/HSZ-AE catalyst. We also noted that the selectivity of ROP and THP products on the Cu/HSZ-IW catalyst was higher than that on the Cu/HSZ-AE catalyst, which might be ascribed to that the relatively weak acidity of Cu/HSZ-AE catalyst suppressed the occurrence of side reactions.

As discussed above, the Cu/HSZ-IW catalyst exhibited the poor stability in the direct conversion of HMF. For the metal-acid bifunctional catalysts, this phenomenon might be due to the deactivation of metal sites or acid sites. In this case, the catalytic performance of Cu/HSZ-IW catalyst in etherification of BHMF with ethanol was tested. As seen in Figure 8a, both the BHMF conversion and BEMF yield were increased at the beginning and then maintained at about 100% and 72~74%, respectively, during the whole testing period. Subsequently, the performance of the used Cu/HSZ-IW catalyst (HMF feeding, reaction at 140 °C for 8 h) was evaluated in the etherification of BHMF by transforming the HMF into BHMF (Figure 8b). It can be seen that after feeding with BHMF, the BEMF yield increased to 73%, which was closing to that observed on the fresh Cu/HSZ-IW catalyst. Thus, for the direct conversion of HMF, the dramatically decrease of BEMF yield observed over the Cu/HSZ-IW catalyst should be attributed to the deactivation of metal sites.

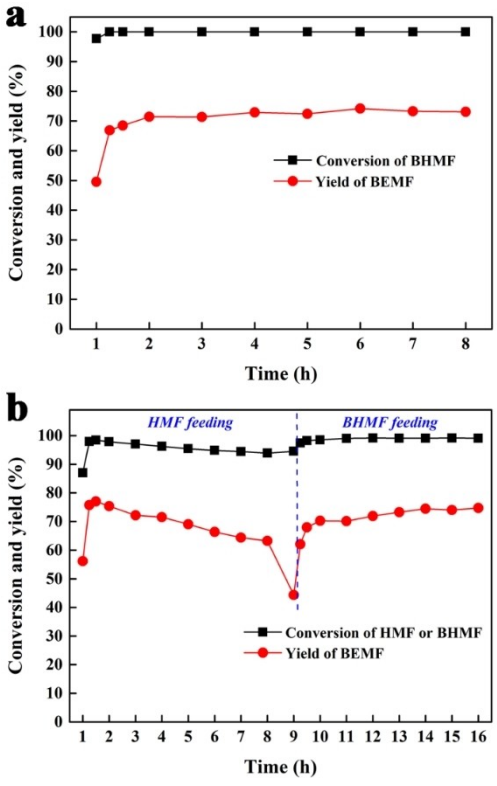

Figure 8. Catalytic performances of the Cu/HSZ-IW catalyst in etherification of BHMF to BEMF. (Reaction conditions: 1.0 g catalyst, 2.0 g L^{-1} BHMF /ethanol, WHSV of BHMF = 0.05 h^{-1}, 2.0 MPa H_2, and 140 °C).

The copper content and particle size distributions of the used catalysts were also characterized by ICP-OES, TEM and N_2 adsorption (Table 4). The results showed that the amount of copper species on the used Cu/HSZ-IW and Cu/HSZ-AE catalysts was 4.79 wt% and 4.74 wt%, which was lower than that of the fresh catalysts. This change was mainly due to the formation of carbon deposition on the catalyst. After adjusting the Cu content by deducting the carbon deposition, the actual content of Cu was almost same to that of the fresh catalysts. Moreover, the average size of the copper particles was also maintained after the reaction (Figure 4S). These results indicated that the leaching of copper species and transmigrating of copper particles during the reaction were negligible. In this case, it was reasonable to deduce that the deactivation of Cu/HSZ-IW catalyst should be due to the inactivation of copper species.

According to the literature, the carbon deposition might be the main reason for the deactivation of the Cu-base catalysts.[31] Then, TG technique was selected to quantitatively analyze the carbon deposition on these catalysts after 8 h reaction time (Figure 5S). As listed in Table 4, the carbon content of Cu/HSZ catalysts was higher than 2.5%, meaning that a small part of HMF or its derivatives was converted into carbon deposition via the polymerization. The decrease in the BET surface area of the used catalyst also confirmed the influenced of carbon deposition on the catalyst from the other side. It is worth noting that the stronger acidity of zeolites could promote generation of carbonaceous deposit.[2] The direct evidence is that the HSZ catalyst which possesses the stronger acidity, has the maximum amount of carbon deposition (3.67%). As compared to the Cu/HSZ-IW catalyst, the acidity of Cu/HSZ-AE catalyst was relatively weaker, which could help to decrease the generate rate of carbon deposition. Moreover, considering the carbon deposition is a slow process, the deactivation of Cu/HSZ-IW catalyst was observed after first 1.5 h, while the Cu/HSZ-AE catalyst maintained the high BEMF yield even though extend the time to 8 h. Hence, it is reasonable to deduce that the carbon deposition tolerance of Cu/HSZ-AE catalyst was higher, which should be attributed to its smaller size of copper particles.

Conclusion

In this work, the direct conversion of HMF to BEMF was investigated in detail over the copper-loaded hierarchically structured ZSM-5 catalyst. The results demonstrated that for the Cu/HSZ catalysts, the main reaction path was that HMF was firstly hydrogenated into BHMF and then the BHMF was etherified to produce BEMF. Moreover, the deactivation of Cu/HSZ catalysts should be attributed to the deposition of carbon species on the copper sites. As compared to the Cu/HSZ-IW catalyst prepared via incipient-wetness impregnation, the Cu/HSZ-AE catalyst prepared by the ammonia evaporation (AE) method exhibited more excellent BEMF yield and stability. This reason could be ascribed to that the AE method facilitated the dispersion of copper particles and reduced the acidity, which in turn improved the hydrogenation activity and carbon deposition tolerance of the catalyst. The results of this work would help to develop efficient metal-acid bifunctional catalyst for the industrial production of BAMF from HMF.

Table 4. Physicochemical properties of the used Cu/HSZ catalysts.

Catalyst	Cu [wt%][a]	d_{Cu} [nm][b]	S_{BET} [$m^2 \cdot g^{-1}$][c]	Carbon deposition [wt%][d]
Cu/HSZ-IW	4.79	2.80	296	3.36
Cu/HSZ-AE	4.74	2.25	304	2.66

[a] Calculated by ICP-OES. [b] Average Cu particle size was calculated by HAADF/STEM images. [c] Determined by BET method. [d] The content of carbon deposition was determined by TG.

Experimental Section

Materials: Ethanol (EtOH, ≥99.7%), tetraethyl orthosilicate (TEOS, $SiO_2 \geq 28.4\%$), copper nitrate trihydrate ($Cu(NO_3)_2 \cdot 3H_2O$, 99%), ammonium hydroxide ($NH_3 \cdot H_2O$, 25%), and tetra-n-propylammonium hydroxide (TPAOH, 25%) were obtained from Sinopharm Chemical Reagent Co., Ltd. (Shanghai, China). Aluminum isopropoxide (AIP, 99.99%), hexadecyltrimethoxysilane (HTS, ≥85%), and 5-ethoxymethylfurfural (EMF, 97%) were purchased from Aladdin Industrial Inc. (Shanghai, China). 5-Hydroxymethylfurfural (HMF, 99%) and 2,5-bis(hydroxymethyl)furan (BHMF, 99%) were provided by Zhejiang Sugar Energy Technology Co., Ltd. (Ningbo, China).

Catalyst synthesis: Hierarchically structured ZSM-5 zeolite (HSZ) was prepared by a dry-gel conversion method. The preparation procedure of the HSZ sample was as follows: Firstly, AIP, TPAOH, and 500 mL of the EtOH were mixed under stirring. After the AIP was completely dissolved to form clear solutions A, TEOS, HTS, and 500 mL of ethanol were successively added to the solutions A to obtain a mixed solution with a molar ratio of $1SiO_2$: $0.005Al_2O_3$: 0.2TPAOH: 0.05HTS: 20EtOH. The mixed solution was then intensely stirred until a homogeneous gel was achieved. Subsequently, the gel was aged in fume cupboard for 5 days at room temperature to obtain the dry gel by evaporating the solvent. Dry gel was added into a 50 mL PTFE inner cup before placed in a Teflon-lined autoclave reactor (250 mL). Moreover, 70 mL of deionized water was added between the two PTFE inner cups. The crystallization was carried out in an oven at 180 °C for 72 h. After crystallization, the obtained product was filtered and washed with deionized water for three times. Then the product was dried in an oven at 100 °C for 12 h and calcined in a muffle furnace at 550 °C for 7 h to obtain the H-form HSZ catalyst.

The HSZ supported Cu catalysts were prepared by incipient-wetness impregnation (IW) and ammonia-evaporation deposition-precipitation (AE), which were denoted as Cu/HSZ-IW, Cu/HSZ-AE, respectively. The nominal Cu loading of these catalysts was 5.0 wt %. Cu/HSZ-IW catalyst was prepared as follows: 1.0 g $Cu(NO_3)_2 \cdot 3H_2O$ was first dissolved in 8 g deionized water. Then, 5 g HSZ was immersed in the solution for 24 h. The obtained solid was dried in an air oven at 100 °C for 24 h and calcined at 480 °C for 10 h.

Cu/HSZ-AE catalyst was synthesized by deposition precipitation using ammonia evaporation. 1.0 g $Cu(NO_3)_2 \cdot 3H_2O$, 60 g deionized water, and 8 mL $NH_3 \cdot H_2O$ were added to a 100 mL three-neck flask. After mechanical stirring (200 rpm) for 10 min, 5 g HSZ was added to flask and then stirred for 4 h at room temperature. The mixture was heated to 90 °C under stirring and hold on 90 °C until the pH value of the suspension decreased to 7. Then, the product was filtered and washed by deionized water for several times. The

obtained solid was dried at 100 °C for 24 h and calcined in air at 480 °C for 10 h.

Catalyst characterization: X-ray diffraction (XRD) patterns were measured with a Bruker D8 ADVANCE X-ray diffractometer using Cu Kα radiation at λ = 0.154 nm. The SEM and TEM images were collected using Thermo Sicentifc Verios G4 UC scanning electronic microscope and ThermoFisher Talos F200X transmission electron microscope, respectively. The compositions of the samples were determined using a Rigaku ZSX Primus II X-ray fluorescence instrument. The N_2 physisorption isotherms at 77 K were measured using a Micromeritics ASAP-2020 instrument. The compositions of the sample were determined by the inductively coupled plasma optical emission spectrometer (ICP-OES).

NH_3 temperature-programmed desorption (NH_3-TPD) of the sample was conducted using a Tianjin XQ TP-5076 instrument equipped with a Hiden QGA mass spectrum detector. 0.1 g of the sample was first reduced at 300 °C for 5 h in the flow of 8% H_2/Ar mixed gas. After the sample was cooled to 100 °C in an Ar gas flow, the 5% NH_3/Ar mixed gas was introduced for 1 h. NH_3 desorption was measured between 100 and 650 °C with a heating rate of 10 °C min^{-1}.

The dispersion of the sample was determined by N_2O chemisorption. The sample was firstly reduced in 8% H_2/Ar mixture at 300 °C for 2 h. The amount of H_2 consumed was monitored by TCD and labeled as A. After the sample was cooled to 50 °C in the flow of Ar, the pure N_2O was introduced for 60 min to oxidize the surface copper atoms. Then, the reduction of surface Cu_2O was conducted in 8% H_2/Ar mixture at 300 °C for 2 h. The amount of H_2 consumed was recorded by TCD and denoted as B. The dispersion (D_{Cu}) of metallic copper, exposed Cu specific surface (S_{Cu}) and copper particle size (d_{Cu}) were calculated from Equations (1)–(3):[27,32]

$$D_{Cu} = (2 \times B)/A \times 100\,\% \quad (1)$$

$$S_{Cu} = (2 \times B \times N_A)/(A \times M_{Cu} \times 1.46 \times 1019) \quad (2)$$

$$d_{Cu} = 6/(S_{Cu} \times \rho_{Cu}) = 0.5 \times A/B \quad (3)$$

where N_A is Avogadro's constant (6.02×10^{23} atoms·mol^{-1}), M_{Cu} is the molar mass of copper (63.546 g·mol^{-1}), 1.46×10^{19} is the number of copper atoms per m^2, and ρ_{Cu} is the density of copper (8.92 g/cm^3).

Pyridine adsorption Fourier-transform infrared (Py-IR) was conducted using a Bruker Vertex 70 FT-IR spectrometer. Firstly, the sample was pressed into a wafer and then heat-treated in an Ar flow (25 mL·min^{-1}) at 400 °C for 1 h. After cooling down to room temperature, the IR spectrum of the sample was recorded. Then, the pyridine was introduced into the cell at room temperature for 1 h. The IR spectrum was collected after evacuation at 350 °C for 1 h.

H_2-TPR of the samples was conducted using an Auto ChemII2920 instrument equipped with a TCD detector. The sample was heat-treated in He flow at 200 °C for 1 h and then cooled to room temperature. A gas mixture of 8% H_2 in He was shifted, and the hydrogen consumption was recorded by TCD from 30 °C to 300 °C with a heating rate of 10 °C min^{-1}.

Thermogravimetry (TG) was evaluated by a Perkin-Elmer Pyris Diamond apparatus using a temperature ramp from 30 to 800 °C with a heating rate of 10 °C min^{-1} in an air atmosphere.

Catalytic activity test:

All evaluation experiments were carried out in a continuous flow fixed bed reactor with a stainless steel tube (8 mm inner diameter). In each test, 1 g of catalyst were diluted using 5.0 g of quartz sand with identical mesh size and then loaded into the middle of the reactor by glass wool. The catalyst was reduced in situ at 300 °C for 5 h in flowing H_2 with a rate of 20 mL·min^{-1}. After the reactor was cooled to the 140 °C, the temperature was maintained at 140 °C and the pressure of H_2 was increased from 0.1 MPa to 2.0 MPa. A mixture of HMF or BHMF and ethanol (HMF concentration of 2 g·L^{-1}) was then fed into the reactor (WHSV = 0.05 h^{-1}) with a co-feeding H_2 flow of 20 mL·min^{-1}. The liquid phase products were collected in the gas-liquid separator using cold trap. The reaction products were periodically extracted from the separator. Qualitative analysis of products was performed using an Agilent 7890B–5977A GC-MS instrument combined with an Agilent DB-wax capillary column. Quantitative analysis of products was performed using an Agilent 1260 HPLC Infinity instrument equipped with an ultraviolet (UV) detector and an Agilent C18 column. Quantitative analysis of HMF and EMF was performed with UV detector at 278 nm, a mixture of trifluoroacetate aqueous solution and methanol [70:30 (v/v)] was used as the mobile phase at a flow rate of 0.8 mL·min^{-1}, and the column temperature was maintained at 40 °C. Quantitative analysis of BHMF, EMFA, and BEMF was performed with UV detector at 220 nm, a mixture of trifluoroacetate aqueous solution and methanol [45:55 (v/v)] was used as the mobile phase at a flow rate of 1.0 mL·min^{-1}, and the column temperature was maintained at 40 °C. The other by-products were analyzed by an off-line gas-chromatography (GC8860, Agilent, USA) using a capillary column DB-wax and an FID detector.

Acknowledgements

This work was financially supported by Zhejiang Provincial Natural Science Foundation of China (LR16B030001, LQ19B060002, LY19B030003), the Key Research Program of Frontier Sciences of CAS (No. QYZDB-SSW-JSC037), K. C. Wong Education Foundation (rczx0800), Fujian Institute of Innovation of Chinese Academy of Sciences (FJCXY18020202), Ningbo Municipal Bureau of Science and Technology (2019B10096, 2019A610029, 2018B10056), Zhejiang Provincial Key Research and Development Program (2021C01062).

Conflict of Interest

The authors declare no conflict of interest.

Keywords: 5-Hydroxymethylfurfural · Hydrogenation · Etherification · 2,5-Bis(ethoxymethyl)furan · Bifunctional catalyst

[1] a) R. A. Sheldon, *Green Chem.* **2014**, *16*, 950–963; b) O. Ellabban, H. Abu-Rub, F. Blaabjerg, *Renewable Sustainable Energy Rev.* **2014**, *39*, 748–764; c) R. R. Chen, J. Y. Xin, D. X. Yan, H. X. Dong, X. M. Lu, S. J. Zhang, *ChemSusChem* **2019**, *12*, 2715–2724.
[2] a) A. A. Rosatella, S. P. Simeonov, R. F. M. Frade, C. A. M. Afonso, *Green Chem.* **2011**, *13*, 754–793; b) Z. Y. Nakagawa, M. Tamura, K. Tomishige, *ACS Catal.* **2013**, *3*, 2655–2668; c) I. Thapa, B. Mullen, A. Saleem, C. Leibig, R. T. Baker, J. B. Giorgi, *Appl. Catal. A* **2017**, *539*, 70–79; d) W.

Cheng, B. Saha, D. G. Vlachos, *ChemSusChem* **2018**, *11*, 3609–3617; e) P. L. Zhang, J. Yang, H. L. Hu, D. X. Hu, J. Gan, Y. X. Zhang, C. L. Chen, X. Q. Li, L. Wang, J. Zhang, *Catal. Sci. Technol.* **2020**, *10*, 4684–4692.
[3] a) E. R. Sacia, M. Balakrishnan, A. T. Bell, *J. Catal.* **2014**, *313*, 70–79; b) J. D. Lewis, S. Van de Vyver, A. J. Crisci, W. R. Gunther, V. K. Michaelis, R. G. Griffin, Y. Román-Leshkov, *ChemSusChem* **2014**, *7*, 2255–2265; c) L. Hu, L. Lin, Z. Wu, S. Y. Zhou, S. J. Liu, *Renewable Sustainable Energy Rev.* **2017**, *74*, 230–257; d) J. N. Wei, X. J. Cao, T. Wang, H. Liu, X. Tang, X. H. Zeng, Y. Sun, T. Z. Lei, S. J. Liu, L. Lin, *Catal. Sci. Technol.* **2018**, *8*, 4474–4484.
[4] a) F. F. Yang, S. G. Zhang, Z. C. Zhang, J. B. Mao, S. M. Li, J. M. Yin, J. X. Zhou, *Catal. Sci. Technol.* **2015**, *5*, 4602–4612; b) G. Raveendra, A. Rajasekhar, M. Srinivas, P. S. S. Prasad, N. Lingaiah, *Appl. Catal. A* **2016**, *520*, 105–113; c) P. Lanzafame, K. Barbera, G. Papanikolaou, S. Perathoner, G. Centi, M. Migliori, E. Catizzone, G. Giordano, *Catal. Today* **2018**, *304*, 97–102.
[5] a) J. Jae, E. Mahmoud, R. F. Lobo, D. G. Vlachos, *ChemCatChem* **2014**, *6*, 508–513; b) H. Nguyen, N. Xiao, S. Daniels, N. Marcella, J. Timoshenko, A. Frenkel, D. G. Vlachos, *ACS Catal.* **2017**, *7*, 7363–7370.
[6] a) Q. Cao, W. Y. Liang, J. Guan, L. Wang, Q. Qu, X. Z. Zhang, X. C. Wang, X. D. Mu, *Appl. Catal. A* **2014**, *481*, 49–53; b) T. A. Natsir, S. Shimazu, *Fuel Process. Technol.* **2020**, *200*, 106308.
[7] a) M. Chatterjee, T. Ishizaka, H. Kawanami, *Green Chem.* **2014**, *16*, 4734–4739; b) J. Han, Y. Kim, B. Y. Jung, S. Y. Hwang, J. Jegal, J. W. Kim, Y. Lee, *RSC Adv.* **2016**, *6*, 93394–93397; c) M. Balakrishnan, E. R. Sacia, A. T. Bell, *Green Chem.* **2012**, *14*, 1626–1634; d) M. Musolino, M. J. Ginés-Molina, R. Moreno-Tost, F. Aricò, *ACS Sustainable Chem. Eng.* **2019**, *7*, 10221–10226; e) Y. F. Zhu, X. Kong, H. Y. Zheng, G. Q. Ding, Y. L. Zhu, Y. W. Li, *Catal. Sci. Technol.* **2015**, *5*, 4208–4217.
[8] D. X. Hu, H. L. Hu, H. Zhou, G. Z. Li, C. L. Chen, J. Zhang, Y. Yang, Y. P. Hu, Y. J. Zhang, L. Wang, *Catal. Sci. Technol.* **2018**, *8*, 6091–6099.
[9] a) H. L. Hu, D. X. Hu, H. T. Jin, P. L. Zhang, G. Z. Li, H. Zhou, Y. Yang, C. L. Chen, J. Zhang, L. Wang, *ChemCatChem* **2019**, *11*, 2179–2186; b) W. T. Fang, H. L. Hu, P. Dong, Z. S. Ma, Y. L. He, L. Wang, Y. J. Zhang, *Appl. Catal. A* **2018**, *565*, 146–151; c) D. X. Hu, H. L. Hu, H. T. Jin, P. L. Zhang, Y. H. Hu, S. H. Ying, X. M. Li, Y. Yang, J. Zhang, L. Wang, *Appl. Catal. A* **2020**, *590*, 117338.
[10] J. Z. Chen, Y. Y. Guo, J. Y. Chen, L. Song, L. M. Chen, *ChemCatChem* **2014**, *6*, 3174–3181.
[11] a) C. Ju, M. R. Li, Y. M. Fang, T. W. Tan, *Green Chem.* **2018**, *20*, 4492–4499; b) Y. Y. Bai, L. Wei, M. F. Yang, H. Y. Chen, S. Holdren, G. H. Zhu, D. T. Tran, C. L. Yao, R. C. Sun, Y. B. Pan, D. X. Liu, *J. Mater. Chem. A* **2018**, *6*, 7693–7705.
[12] J. N. Wei, T. Wang, X. J. Cao, H. Liu, X. Tang, Y. Sun, X. H. Zeng, T. Z. Lei, S. J. Liu, L. Lin, *Appl. Catal. B* **2019**, *258*, 117793.
[13] a) N. Künzle, R. Hess, T. Mallat, A. Baiker, *J. Catal.* **1999**, *186*, 239–241; b) S. Lima, D. Chadwick, K. Hellgardt, *RSC Adv.* **2017**, *7*, 31401–31407.
[14] H. V. Koningsveld, J. C. Jansen, H. V. Bekkum, *Zeolites* **1990**, *10*, 235–242.
[15] S. Goodarznia, K. J. Smith, *J. Mol. Catal. A* **2010**, *320*, 1–13.
[16] K. K. Zhu, J. M. Sun, J. Liu, L. Q. Wang, H. Y. Wan, J. Z. Hu, Y. Wang, C. H. F. Peden, Z. M. Nie, *ACS Catal.* **2011**, *1*, 682–690.
[17] a) A. Bansode, B. Tidona, P. R. von Rohr, A. Urakawa, *Catal. Sci. Technol.* **2013**, *3*, 767–778; b) C. Z. Li, J. S. Ma, Z. H. Xiao, S. B. Hector, R. K. Liu, S. M. Zuo, X. F. Xie, A. H. Zhang, H. Wu, Q. Liu, *Fuel* **2018**, *218*, 59–66.
[18] a) N. Suárez, J. Pérez-Pariente, F. Mondragón, A. Moreno, *Microporous Mesoporous Mater.* **2019**, *280*, 144–150; b) L. Chen, X. M. Zhang, Q. Han, L. J. Xu, S. Y. Zhang, Y. Y. Yuan, L. Xu, *Appl. Catal. A* **2020**, *598*, 117588.
[19] K. H. Chung, D. R. Chang, B. G. Park, *Bioresour. Technol.* **2008**, *99*, 7438–7443.
[20] S. Wang, Z. Huang, Y. J. Luo, J. H. Wang, Y. Fang, W. M. Hu, Y. H. Yue, H. L. Xu, W. Shen, *Catal. Sci. Technol.* **2020**, *10*, 6562–6572.
[21] H. Wang, R. N. Xu, Y. Jin, R. D. Zhang, *Catal. Today* **2019**, *327*, 295–307.
[22] a) M. Bjørgen, F. Joensen, M. S. Holm, U. Olsbye, K. Lillerud, S. Svelle, *Appl. Catal. A* **2008**, *345*, 43–50; b) K. Sadowska, A. Wach, Z. Olejniczak, P. Kuśtrowski, J. Datka, *Microporous Mesoporous Mater.* **2013**, 82–88; c) S. J. You, E. D. Park, *Microporous Mesoporous Mater.* **2014**, *186*,121–129.
[23] a) C. A. Emeis, *J. Catal.* **1993**, *141*, 347–354; b) H. L. Hu, J. H. Lyu, J. Y. Rui, J. Cen, Q. F. Zhang, Q. T. Wang, W. W. Han, X. N. Li, *Catal. Sci. Technol.* **2016**, *6*, 2647–2652.
[24] a) F. Benaliouche, Y. Boucheffa, P. Ayrault, S. Mignard, P. Magnoux, *Microporous Mesoporous Mater.* **2008**, *111*, 80–88; b) S. R. Wang, W. W. Guo, L. J. Zhu, H. X. Wang, K. Z. Qiu, K. F. Cen, *J. Phys. Chem. C* **2015**, *119*, 524–533.
[25] H. W. Zhang, H. R. Tan, S. Jaenicke, G. K. Chuah, *J. Catal.* **2020**, *389*, 19–28.
[26] C. C. Chen, L. Lin, R. P. Ye, M. L. Sun, J. X. Yang, F. Li, Y. G. Yao, *J. Catal.* **2020**, *389*, 421–431.
[27] H. Du, X. Y. Ma, P. F. Yan, M. Jiang, Z. Zhao, Z. C. Zhang, *Fuel Process. Technol.* **2019**, *193*, 221–231.
[28] F. F. Cai, W. Zhu, G. M. Xiao, *Catal. Sci. Technol.* **2016**, *6*, 4889–4900.
[29] J. Florek-Milewska, P. Decyk, M. Ziolek, *Appl. Catal. A* **2011**, *393*, 215–224.
[30] a) R. Alamillo, M. Tucker, M. Chia, Y. Pagán-Torres, J. Dumesic, *Green Chem.* **2012**, *14*, 1413–1419; b) A. Iriondo, A. Mendiguren, M. B. Güemez, J. Requies, J. F. Cambra, *Catal. Today* **2017**, *279*, 286–295.
[31] a) Y. F. Zhu, X. Kong, H. Y. Zheng, G. Q. Ding, Y. L. Zhu, Y. W. Li, *Catal. Sci. Technol.* **2015**, *5*, 4208–4217; b) B. S. Solanki, C. V. Rode, *Green Chem.* **2019**, *21*, 6390–6406; c) K. T. V. Rao, Y. L. Hu, Z. S. Yuan, Y. S. Zhang, C. B. C. Xu, *Appl. Catal. A* **2021**, *609*, 117892.
[32] S. X. Xia, R. F. Nie, X. Y. Lu, L. Wang, P. Chen, Z. Y. Hou, *J. Catal.* **2012**, *296*, 1–11.

Manuscript received: April 3, 2021
Revised manuscript received: May 10, 2021
Version of record online: ■■, ■■■

FULL PAPERS

Bifunctional catalyst: The highly-efficient conversion of 5-hydroxymethylfurfural (HMF) to 2,5-bis(ethoxymethyl)furan (BEMF) was achieved by using the copper-loaded hierarchically structured ZSM-5 (Cu/HSZ) catalysts in the continuous fixed-bed reactor.